SMART 2025

July 1-3, 2025, Linz, Austria

Chairmen: Michael Krommer
Manfred Nader
Martin Schagerl

Kurtis Y., Kosikova A., Vlachas K., Ferrari R., Smyth A.W., Chatzi E. (2025) *Monitoring-based Identification of Corrosion in Steel Structures.* In Proc. of **11th ECCOMAS Thematic Conference on Smart Structures and Materials (SMART 2025)**, M. Krommer, M. Nader, M. Schagerl and A. Benjeddou (Eds.), Johannes Kepler University Linz (JKU Linz), Linz, Austria, July 1-3, 2025, Accepted 7 September 2025, Part I, SS 02 - SHM-Informed Strategies and Their Use for Lifetime Extension of Structures, Luis David Avendaño-Valencia, Stefano Manzoni, pp. 41–52. https://www.jku.at/en/institute-of-technical-mechanics-tmech/events-1/smart-2025/proceedings/

Part I
SS 02 - SHM-INFORMED STRATEGIES AND THEIR USE FOR LIFETIME EXTENSION OF STRUCTURES

Luis David Avendaño-Valencia
Stefano Manzoni

XI ECCOMAS Thematic Conference on Smart Structures and Materials - SMART 2025
M. Krommer, M. Nader and M. Schagerl (Eds)

Received: 14 May 2025 / Revised: 25 August 2025 / Accepted: 7 September 2025
© The Author(s) 2025

Monitoring-based Identification of Corrosion in Steel Structures

Yasemin Kurtis, Antonina Kosikova, Konstantinos Vlachas, Rosalba Ferrari, Andrew W. Smyth, Eleni Chatzi

Abstract. *Over the service lifetime of a structure, corrosion in steel components progressively deteriorates their load-bearing capacity and compromises overall structural safety. Despite its substantial impact on structural performance, research on corrosion progression and its long-term effects remains limited. Most existing studies focus on corrosion incidents in reinforced concrete bars and steel cables, while effective methods for corrosion detection in steel members, such as girders and other structural elements are scarce. This study presents a methodology for detection and quantification of corrosion-induced damage in large-span steel structural components. The proposed approach leverages measured strain data from the monitored structure and employs a probabilistic framework to model and assess the progression of corrosion over time. Corrosion localization is achieved via use of a data-driven indicator, relying on transmittance functions, which are inferred from pairwise strain measurements at locations within the structure. To address the challenge of limited sensor measurements, a Gaussian Process Regression (GPR) model is employed to predict strains at unmeasured locations. The method is validated through numerical simulations employing a high-fidelity finite element model of a steel bridge.*

Key words: Corrosion in Steel Structures, Structural Health Monitoring, Finite Element Model

Yasemin Kurtis & Konstantinos Vlachas & Eleni Chatzi
Department of Civil, Environmental and Geomatic, ETH Zurich, Zürich, 8092, Switzerland
e-mail: ykurtis@studnet.ethz.ch

Antonina Kosikova & Andrew W. Smyth
Civil Engineering and Engineering Mechanics, Columbia University, New-York, NY, 10027-6699, U.S.A.
e-mail: ak4967@columbia.edu

Rosalba Ferrari
Department of Engineering and Applied Sciences, University of Bergamo, Dalmine, BG, 24044, Italy
e-mail: rosalba.ferrari@unibg.it

1 INTRODUCTION

Steel bridges constitute essential components of transportation infrastructure systems but are inherently prone to corrosion-induced degradation, which progressively diminishes structural capacity and incurs significant maintenance expenditures. Conventional inspection techniques, including visual assessment and non-destructive evaluation (NDE) methods such as ultrasonic testing and eddy current inspection, exhibit fundamental limitations in sensitivity and spatial resolution, particularly when applied to the early detection of corrosion in regions characterized by complex geometrical configurations [1, 2]. Advanced image-based inspection techniques, such as infrared thermography, enhance corrosion detection capabilities, but their efficacy remains limited in regions that are difficult to access [3]. Vibration-based monitoring provides an automated framework for continuous, long-term assessment of structural integrity [4]. This approach relies on identifying alterations in the dynamic response of a structure, such as reductions in stiffness and changes in damping behavior, as indirect indicators of damage. However, the assessment is often limited to identifying updated modal parameters, such as natural frequencies or mode shapes, with respect to a reference state, without explicitly linking these changes to specific physical deterioration mechanisms. In particular, the relationship between corrosion-induced material loss and the consequent reduction in structural stiffness in steel systems remains insufficiently explored, despite stiffness degradation being a primary contributor to structural failure in these structures. Existing studies are primarily focused on evaluating the impact of corrosion on structural behavior and performance characteristics, rather than providing methodologies for real-time quantification of the corrosion severity [5, 6]. Furthermore, much of the existing literature concentrates specifically on reinforced concrete elements and steel cables, while steel girders and arch structures remain underinvestigated in the context of corrosion-induced stiffness degradation [7, 8]. Consequently, a significant gap remains in the real-time monitoring and quantification of corrosion progression for the in-service steel structures. This study aims to address this gap through a strain-based probabilistic framework capable of identifying both the location and severity of corrosion in steel structures, based on analysis of the strain measurements. The proposed methodology comprises three key stages: First, damage localization is achieved using transmittance functions, which capture alterations in the strain response to identify affected regions. Second, strain prediction at uninstrumented locations is performed using Gaussian Process Regression (GPR), a probabilistic machine learning technique that reconstructs strain fields based on measurements from a sparse sensor network. Finally, the depth of corrosion is estimated through an inverse problem, where the maximum likelihood estimate (MLE) is used to determine the most probable depth of corrosion penetration based on strain measurements. The methodology is validated through numerical simulations using a high-fidelity finite element method (FEM) model of the Paderno d'Adda Bridge, as illustrated in Figure 1. The proposed approach is systematically tested under both uniform and pitting corrosion scenarios, assessing its capability to accurately localize damaged regions and quantify corrosion penetration depth across varying damage conditions.

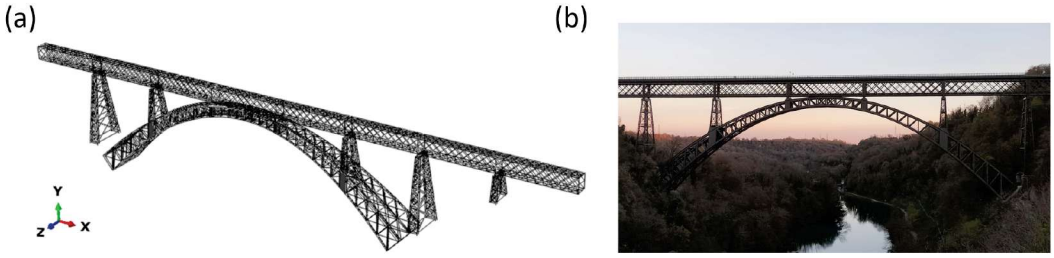

Figure 1: *(a) Finite Element Model. (b) Paderno d'Adda Bridge.*

2 DESCRIPTION OF THE MODEL

The FEM model of the Paderno d'Adda Bridge, originally developed in [9], was used in this study. The model, assembled in Abaqus using Euler-Bernoulli beam elements, represents the bridge's truss frame including the parabolic arch, piers, and upper girder deck. Geometric and boundary condition data were obtained from original design drawings archived in the Archivio Storico Nazionale di Torino. Built-in constraints were applied at the arch shoulders and pier bases, with roller supports at the upper beam bearings. The model comprises 5,337 beam elements and 12,794 nodes, resulting in 13,444 degrees of freedom. In this study, uniform material properties were assigned to the main structural components. A Young's modulus of 204 GPa and a Poisson's ratio of 0.30 were used for all components, while the mass density varied: 8.19 g/cm^3 for the arch, 14.5 g/cm^3 for the girders, and 1.03 g/cm^3 for the piles.

To simulate operational conditions, a dynamic train load was applied following the approach proposed in [10]. It was implemented as a repeating sequence of one second unloaded and one second loaded conditions, using concentrated forces of 19.27 kN at each girder node, determined based on historical loading conditions [11]. This type of loading represents an idealized, periodic train-passing scenario. While it does not reflect exact axle passage intervals, it allows for studying the structure's response to alternating loads under consistent timing. Strain data were collected at 100 Hz during 20 seconds of loading and 80 seconds of free vibration. To simulate structural degradation, both uniform and pitting corrosion cases were simulated in the FEM model. The arch and girder elements were selected for analysis due to their increased exposure to environmental stressors, such as proximity to the water surface, and their susceptibility to high strain concentrations resulting from cyclic traffic loading [12], [13]. Uniform corrosion is modeled as a distributed reduction in T-beam flange thickness over extensive regions of the upper and lower arch chords, representing generalized material degradation resulting from prolonged corrosive exposure [14]. Pitting corrosion was modeled as a series of localized cross-sectional reductions confined to 5 *cm*-wide regions near girder joints. These regions were chosen to reflect areas of increased vulnerability, such as joints and welds, where corrosion is often initiated and accelerated due to crevice effects, moisture retention, and stress concentration. The simulated pits represent localized material degradation, capturing the irregular and severe nature of pitting typically observed in in-service steel structures [6, 15].

3 METHODOLOGY

3.1 Damage Location Identification

The adopted damage localization approach is based on the use of transmittance functions as a data-driven indicator to identify the corroded regions. The transmittance function (TF) $T_{ij}^{\epsilon}(\omega)$ is defined as the ratio of the cross-spectral density (CSD) over the power spectral density (PSD) at the reference location [16]:

$$T_{ij}^{\epsilon}(\omega) = \frac{G_{ij}^{\epsilon}(\omega)}{G_{jj}^{\epsilon}(\omega)} \tag{1}$$

where $G_{ij}^{\epsilon}(\omega)$ is the CSD function of the strains between locations i and j, and $G_{jj}^{\epsilon}(\omega)$ is the PSD of the strains at location j. This formulation allows for capturing the dynamic relationship between strain responses, making it an effective output-only indicator for structural condition assessment [16]. To enhance sensitivity to damage, the TF is computed within an isolated frequency band corresponding to the natural frequencies of the bridge, as shown in Figure 2(a). The analysis is based exclusively on strain data recorded during the structure's free vibration response after the train passing. To quantify changes in the TF between the healthy and corroded states, a Damage Indicator (DI) is employed, following the formulation introduced in [17]. While originally developed for transmissibility functions, the DI is here adapted to assess strain-based TF variations associated with corrosion-induced damage and defined as:

$$DI_{ij} = \frac{\int_{\omega_1}^{\omega_2} |T_{ij}^{h}(\omega) - T_{ij}^{d}(\omega)| \mathrm{d}\omega}{\int_{\omega_1}^{\omega_2} |T_{ij}^{h}(\omega)| \mathrm{d}\omega} \tag{2}$$

where $T_{ij}^{h}(\omega)$ is the TF for the healthy and $T_{ij}^{d}(\omega)$ the TF for the damaged state, and $[\omega_1, \omega_2]$ corresponds to the selected frequency band.

3.2 Strain predictions at unmeasured locations

To address the common constraint of limited sensor availability in real-world monitoring systems, the proposed methodology incorporates GPR to predict strain values at uninstrumented locations. The strains of the healthy (undamaged) state of the bridge are computed from the calibrated FEM model, providing a comprehensive baseline. For the corroded state, strain measurements are restricted to a subset of locations corresponding to installed sensors, simulating sparse spatial coverage. The GPR model was trained on healthy-state strain data, using sensor node strains as input features and strains at unmeasured locations as output. Training involved maximizing the likelihood under a multivariate normal distribution, given by:

$$P(\epsilon_{\text{obs}}(t)|X) = N\big(\epsilon_{\text{obs}}(t) \mid X, K(X, X'; \boldsymbol{\theta})\big), \quad \text{with} \quad \boldsymbol{\theta} = \left[\sigma_l^2, \sigma_f^2, \sigma_n^2\right] \tag{3}$$

where $\epsilon_{\text{obs}}(t)$ is the vector of observed strain values at the selected node, extracted from the calibrated FEM model in the healthy state, which corresponds to the unmeasured location in the

monitored real-world structure and X is the matrix of input data corresponding to the observed strains at reference nodes in the healthy state. The $K(X, X'; \boldsymbol{\theta})$ is the kernel-covariance matrix of the training inputs where $\boldsymbol{\theta}$ denotes the vector of kernel hyperparameters: length scale, signal variance and noise variance. The trained model was then employed to predict unmeasured strain values at the corroded element as:

$$\epsilon_{\text{obs}}(t^*) = K(X^*, X'; \hat{\boldsymbol{\theta}}) \left[K(X, X'; \hat{\boldsymbol{\theta}})\right]^{-1} \epsilon_{\text{obs}}(t) \tag{4}$$

where $K(X^*, X'; \hat{\boldsymbol{\theta}})$ is the covariance matrix between the new inputs X^* (strains at the reference nodes in the corroded structure) and the training inputs X with $\hat{\boldsymbol{\theta}}$ being the optimal kernel function parameters learned during the training step. The Matérn 3/2 kernel, combined with a stationary kernel to account for measurement noise, was selected as the most suitable candidate based on preliminary analysis of strain cross-correlation functions. This composite kernel is defined as:

$$k(x_i, x_j \mid \boldsymbol{\theta}) = \sigma_f^2 \left(1 + \sqrt{3}\frac{r_{ij}}{\sigma_l^2}\right) \exp\left(-\sqrt{3}\frac{r_{ij}}{\sigma_l^2}\right) + {\sigma_n}^2 I, \tag{5}$$

where r_{ij} is the Euclidean distance between the locations x_i and x_j; the ${\hat{\sigma_n}}^2$ represents the measurement noise variance and I is an identity matrix.

3.3 Corrosion Depth Estimation

Once strain time histories are obtained at both measured and predicted locations, an inverse problem is formulated to estimate the severity of corrosion by quantifying the depth of material penetration. This formulation enables the characterization of corrosion intensity based on deviations from the expected structural response. The observed strain values correspond to the measured data at the sensor locations in the corroded state obtained from the FEM model. The predicted strain values are derived from a force-based strain formulation of a linear system subjected to both axial and bending effects, while incorporating changes in cross-sectional properties and the moment of inertia as a function of corrosion depth d. The relationship is expressed as:

$$\epsilon_{\text{pred}}(t; d) = \frac{F(t)}{EA(d)} + \frac{c(d)M(t)}{EI(d)} \tag{6}$$

where $F(t)$ and $M(t)$ denote the axial force and bending moment as functions of time, extracted from a calibrated FEM model; E is the Young's modulus of the material; $c(d)$ is the distance to the element neutral axis; $A(d)$ is the cross-sectional area, and $I(d)$ is the moment of inertia —expressed as functions of the corrosion depth penetration d. For this study, Bayes' theorem with a non-informative prior was employed as :

$$P(d \mid \{\epsilon_{\text{obs}}(t)\}) \propto P(\{\epsilon_{\text{obs}}(t)\} \mid d) \tag{7}$$

By systematically evaluating the strain response for a range of potential corrosion depths, the method identifies the depth value that maximizes the likelihood of the observed data. The posterior probability $P(d \mid \{\epsilon_{\text{obs}}(t)\})$ of the corrosion depth is considered to be proportional to the likelihood $P(\{\epsilon_{\text{obs}}(t)\} \mid d)$ of the observed strain time-history given the corrosion depth d. Assuming independent and identically distributed (i.i.d.) measurements, the likelihood is formulated as:

$$P(\{\epsilon_{\text{obs}}(t)\} \mid d) = \prod_{t=0}^{N} \frac{1}{\sqrt{2\pi\sigma^2}} \exp\left(-\frac{(\epsilon_{\text{obs}}(t) - \epsilon_{\text{pred}}(t;d))^2}{2\sigma^2}\right) \tag{8}$$

where $\epsilon_{\text{obs}}(t)$ represents the observed strain at time t; $\epsilon_{\text{pred}}(t;d)$ is the predicted strain-time history, estimated according to Eq.(6), the σ^2 is the variance of the time-history of the residuals between $\epsilon_{\text{obs}}(t)$ and $\epsilon_{\text{pred}}(t;d)$, and N corresponding to the size of the datasets. Given the simplified strain formulation, discrepancies between the predicted and measured strain values may arise due to modeling assumptions inherent in the FEM representation. To account for such discrepancies, a modeling error term is incorporated into the formulation, ensuring a more robust and reliable estimation of corrosion severity. This error is computed as the difference between the measured and predicted strains in the healthy state and is assumed to remain constant when propagated to the corroded state.

It is important to emphasize that the adoption of a probabilistic approach, rather than direct estimation of corrosion depth from observed strain, facilitates the quantification of epistemic uncertainty, or degree of belief, in the inferred values. This enhances the framework's applicability to structural health monitoring by providing confidence bounds on the estimated corrosion severity. However, the method relies heavily on the following two assumptions. First, it presumes that loading conditions remain consistent between the healthy and corroded states. In this study, a single train passage is employed as the representative loading scenario. Second, it assumes that the structure exhibits linear elastic behavior, wherein axial strains are linearly proportional to axial forces, and bending strains are linearly proportional to bending moments, in accordance with Hooke's Law.

4 METHODOLOGY APPLICATION

The following section demonstrates the application of the proposed strain-based methodology on the FEM model of the Paderno d'Adda Bridge. Initial evaluations were performed for two severe cases: a 25 *mm* bottom flange reduction representing uniform corrosion, and a 31 *mm* reduction representing pitting corrosion. The methodology's was further assessed under realistic conditions, accounting for prediction uncertainty and measurement noise. Finally, sensitivity to varying corrosion severities is examined.

4.1 Damage Location Identification

Damage location identification was performed using the transmittance-based DI for both uniform and pitting corrosion cases. The frequency band used for the TF computation is

illustrated in Figure 2(a). The sensor locations are presented in Figure 2(b). The DI was computed for multiple possible combinations of sensors and the corresponding evaluation is presented in Figures 2(c),(d).

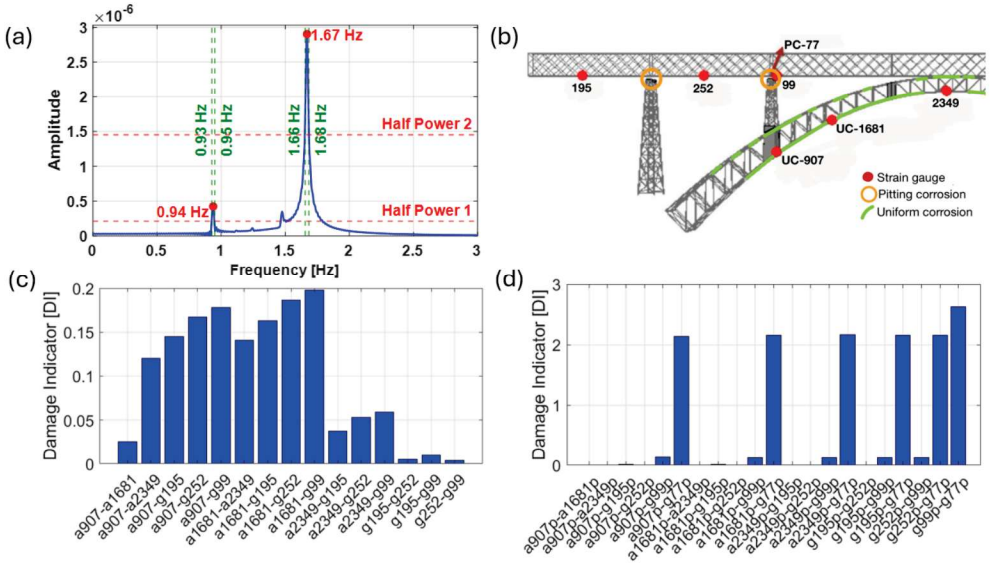

Figure 2: *(a) Frequency band determination. (b) Sensor locations. Sensors placed within the uniform corrosion zone are labeled with the prefix 'UC', while those located in pitting corrosion zones are denoted by 'PC'. (c) DI-values for uniform corrosion. Node combinations are labeled using structural prefixes: 'a' indicate nodes on the arch and 'g' for the girder. (d) DI-values for pitting corrosion. The same prefix convention applies as in (c), with the additional suffix 'p' indicating nodes subjected to pitting corrosion.*

For uniform corrosion, the computed DI values indicate that all sensor combinations involving only the girder nodes exhibit low values, suggesting that the girder remains in a healthy condition. Similarly, combinations between girder nodes and the uncorroded arch node 2349 yield low DI values, indicating that node 2349 is in a healthy state. In contrast, sensor combinations involving either node 907 or node 1681 show significantly higher DI values, suggesting that these locations are likely damaged. Additionally, the DI value between nodes 907 and 1681 remains low, implying that, while both nodes are affected by corrosion, their transmittance remains unchanged. This behavior suggests a similar level of degradation at both nodes and in the surrounding area, indicating that the damage likely extends between the two sensor locations. These results demonstrate that transmittance analysis successfully localizes damage by identifying areas with significant changes in strain response. However, in practical applications, where the exact damage location is unknown, the consistently low DI across girder sensors would indicate that the girder is largely unaffected. This would shift the focus to the arch as the

primary area of concern. Furthermore, the broader distribution of high DI values indicates that uniform corrosion affects a wider region of the structure, rather than being limited to specific locations. In contrast, the DI values for pitting corrosion, reveal a highly localized response. The highest DI is observed at PC-77, which is positioned directly within the pitting corrosion region. A smaller increase in DI is detected at sensor 99, which is located near the pit, while all other sensor locations exhibit negligible DI values. This pattern indicates that the transmittance changes are concentrated around the pit, with minimal impact on the surrounding structure. This localized response is consistent with the expected behavior of pitting corrosion, which generates highly concentrated stress variations. In contrast, the uniform corrosion case exhibits a broad spatial distribution of elevated DI values. The stark difference in DI distribution profiles, broad and diffuse for uniform corrosion versus sharply localized for pitting corrosion, underscores the potential of transmittance-based analysis to differentiate between corrosion types affecting structural elements.

4.2 Estimation of the corrosion depths at measured locations

Following the identification of the corrosion location, the severity of the damage can be subsequently estimated through the probabilistic framework. For the uniform case, the method accurately identifies corrosion depths close to the actual value of 25 *mm* for node 1681 within the damaged area (Figure 3(a)), particularly, the estimation has a relative error of 2.04%. For node 2349, located in the uncorroded region, the method infers a negative value as the corrosion depth (Figure 3(b)). Although this result may seem counterintuitive, it reflects forces redistribution due to adjacent damage, effectively indicating nearby corrosion, while confirming that the node itself remains healthy.

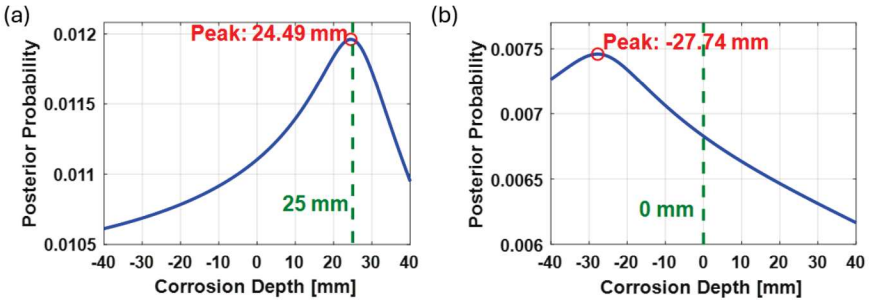

Figure 3: *Uniform corrosion: (a) 1681 (corroded). (b) 2349 (uncorroded).*

The results for the pitting corrosion depth identification are presented in Figure 4. Node 77 is located directly at the pit, while node 99 is located nearby in the uncorroded area. For node 77 the estimated corrosion depth slightly overestimates the actual depth corresponding to a relative error of 14.74%. At node 99, the method effectively indicating a corrosion depth near zero and captures the likelihood of the absence of corrosion at this location.

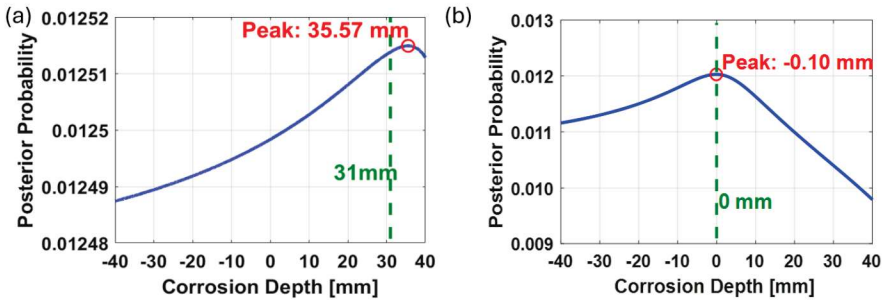

Figure 4: *Pitting corrosion: (a) 77 (corroded). (b) 99 (uncorroded).*

4.3 Estimation of the corrosion depths at unmeasured locations

To evaluate the affect of predicted strains for corrosion depth identification, Node 1447 was selected for analysis. This node lies within the corroded region identified through transmittance analysis but was not instrumented with a sensor, thereby allowing assessment of the method's performance using strain values inferred through GPR using two measured neighboring nodes as the input features (Figure 6(a)). The predicted strains for node 1447 are plotted against the reference FEM strains in Figure 5(a) and the uncertainty of the predictions is shown in a magnified window in Figure 5(b).

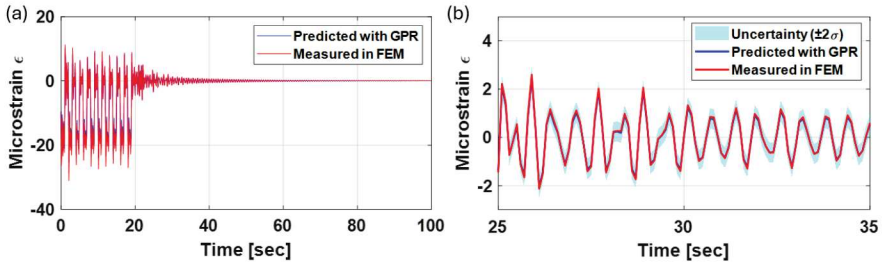

Figure 5: *(a) GPR predicted strain-time history. (b) Uncertainty quantification.*

To quantify the influence of strain prediction under different instrumental conditions, three cases were considered. First, a reference case was established by using FEM strain data for both healthy and corroded states, treating the node as if it was measured directly. In the second scenario, FEM strain data from two reference nodes was used for the healthy state, while GPR was applied to predict corroded-state strains at the unmeasured node. Finally, the measurements noise was added to the reference nodes strain time-histories used for the GPR predictions. The noise was introduced as Gaussian White Noise, equivalent to 10% of the root mean square (RMS) of the measured strain signals.

The results, shown in Figure 6, indicate that while the method allows us to successfully detect corrosion at the unmeasured location, the accuracy decreases. The relative error in the estimation

of the depth of corrosion increases from 5.96% when using FEM strains to 12.84% with GPR predicted strains, which underscores the method's sensitivity to the accuracy of strain data. The introduction of noise further increases the estimation error by approximately 2%, highlighting the compounding effect of measurement noise and prediction errors. Despite these challenges, the method provides corrosion depth estimates close to the actual values, demonstrating its applicability for real-world scenarios.

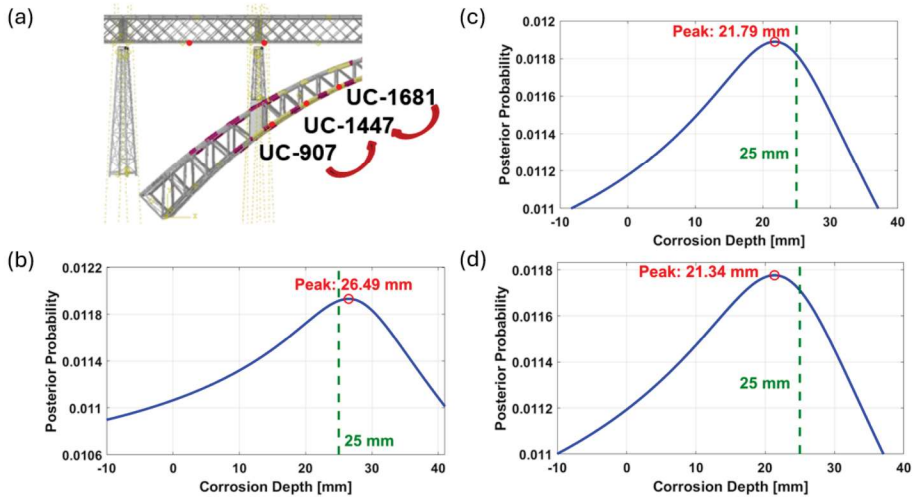

Figure 6: *(a) Unmeasured location (node 1447), and the neighboring locations (nodes 907 and 1681) used for the GPR prediction. Prefix 'UC' stands for uniform corrosion. (b) 1447-Measured. (c) 1447-Predicted. (d) 1447-Predicted based on the noisy strain measurements.*

4.4 Sensitivity to different corrosion stages

To realistically model corrosion, its progression over time must be considered. The corrosion loss for unprotected steel is typically described by an exponential function. Based on the bridge location in Lombardy, Italy, the corrosion is assumed to follow a low degradation rate:

$$C = C_A t^{C_B} = 0.034 t^{0.65} \tag{9}$$

where C is the average corrosion penetration in mm, t is the exposure time in years and C_A, C_B are environment-dependent parameters. For the first 12 years, the corrosion rate is set to zero, accounting for protective coatings delaying material loss [12]. The accumulated section loss (Figure 7(b)) is derived from the time-dependent corrosion rate (Figure 7(a)). Initially, a section loss of 25 mm, corresponding to 100 years, was implemented to assess the methodology. To further evaluate its performance under different levels of material deterioration, additional uniform corrosion stages were introduced, corresponding to section losses of 8 mm at 50 years, 15 mm at 75 years, and 35 mm at 125 years. The results are shown in Figure 7(c).

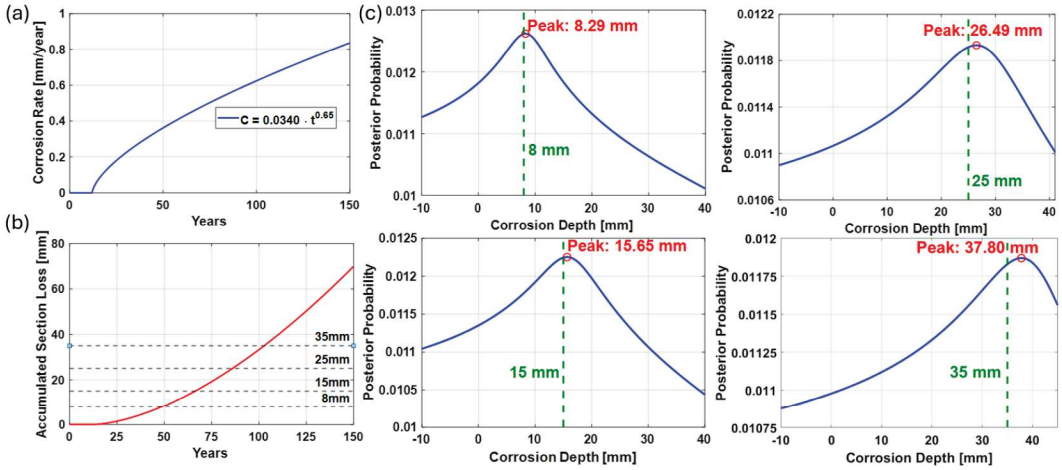

Figure 7: *(a) Corrosion Rate. (b) Accumulated Section loss. (c) Depth Estimation node 1447 for different corrosion stages.*

5 CONCLUSION

This study introduces a strain-based methodology for the detection and quantification of corrosion in steel structures, demonstrated through a case study on a steel arch bridge. The proposed approach effectively identified damage locations and estimated corrosion depths for both uniform and pitting corrosion scenarios. The findings highlight the method's sensitivity to different stages of corrosion, the accuracy of strain prediction at uninstrumented locations, and the influence of measurement noise on the reliability of corrosion assessment. Future work will focus on incorporating force redistribution effects and stiffness degradation to relax the assumption of identical internal forces in healthy and corroded states, thereby enhancing the method's applicability and robustness for real-world structural health monitoring.

REFERENCES

[1] D. Xu, W. Zhang, L. Han, X. Liu, and W. Hu, "Application of Sensor Path Weighting RAPID Algorithm on Pitting Corrosion Monitoring of Aluminum Plate," *Mater.*, vol. 15, no. 11, 2022. [Online]. Available: https://www.mdpi.com/1996-1944/15/11/3887

[2] V. Vasagar, M. K. Hassan, A. M. Abdullah, A. V. Karre, B. Chen, K. Kim, N. Al-Qahtani, and T. Cai, "Non-Destructive Techniques for Corrosion Detection: A Review," *Corros. Eng. Sci. Technol.*, vol. 59, no. 1, pp. 56–85, 2024. [Online]. Available: https://doi.org/10.1177/1478422X241229621

[3] H. J. Lim, S. Hwang, H. Kim, and H. Sohn, "Steel Bridge Corrosion Inspection With Combined Vision and Thermographic Images," *Struct. Health Monit.*, vol. 20, no. 6, pp. 3424–3435, 2021. [Online]. Available: https://doi.org/10.1177/1475921721989407

[4] O. Avci, O. Abdeljaber, S. Kiranyaz, M. Hussein, M. Gabbouj, and D. J. Inman, "A Review of Vibration-Based Damage Detection in Civil Structures: From Traditional Methods to Machine

Learning and Deep Learning Applications," *Mech. Syst. Signal Process.*, vol. 147, p. 107077, 2021. [Online]. Available: https://www.sciencedirect.com/science/article/pii/S0888327020304635

[5] I.-T. Kim, D. K. Dao, Y.-S. Jeong, J. Huh, and J.-H. Ahn, "Effect of Corrosion on the Tension Behavior of Painted Structural Steel Members," *J. Constr. Steel Res.*, vol. 133, pp. 256–268, 2017. [Online]. Available: https://www.sciencedirect.com/science/article/pii/S0143974X1730158X

[6] S. Guo, R. Si, Q. Dai, Z. You, Y. Ma, and J. Wang, "A Critical Review of Corrosion Development and Rust Removal Techniques on the Structural/Environmental Performance of Corroded Steel Bridges," *J. Clean. Prod.*, vol. 233, pp. 126–146, 2019. [Online]. Available: https://www.sciencedirect.com/science/article/pii/S0959652619319766

[7] K. Andisheh, A. Scott, and A. Palermo, "Modeling the Influence of Pitting Corrosion on the Mechanical Properties of Steel Reinforcement," *Mater. Corros.*, vol. 67, no. 11, pp. 1220–1234, 2016. [Online]. Available: https://onlinelibrary.wiley.com/doi/abs/10.1002/maco.201508795

[8] M. J. D. Sloane, R. Betti, G. Marconi, A. L. Hong, and D. Khazem, "Experimental Analysis of a Nondestructive Corrosion Monitoring System for Main Cables of Suspension Bridges," *J. Bridge Eng.*, vol. 18, no. 7, pp. 653–662, 2013. [Online]. Available: https://ascelibrary.org/doi/abs/10.1061/%28ASCE%29BE.1943-5592.0000399

[9] R. Ferrari, G. Cocchetti, and E. Rizzi, "Reference structural investigation on a 19th-century arch iron bridge loyal to design-stage conditions," *International Journal of Architectural Heritage*, vol. 14, no. 10, pp. 1425–1455, 2020. [Online]. Available: https://doi.org/10.1080/15583058.2019.1613453

[10] Z. Zhang, B. Zeng, C. Dai, and W. He, "Study on Structural Service Performance of Heavy-Haul Railway Tunnel with Voided Base," *Adv. Civ. Eng.*, vol. 2018, no. 1, p. 3510979, 2018. [Online]. Available: https://doi.org/10.1155/2018/3510979

[11] R. Ferrari, M. Facheris, and E. Rizzi, "Structural Analysis of the Paderno d'Adda Bridge (Italy, 1889)," *Adv. Mater. Res.*, vol. 133-134, pp. 459–465, 2010. [Online]. Available: https://doi.org/10.4028/www.scientific.net/AMR.133-134.459

[12] W. Zhang and H. Yuan, "Corrosion Fatigue Effects on Life Estimation of Deteriorated Bridges under Vehicle Impacts," *Eng. Struct.*, vol. 71, pp. 128–136, 2014. [Online]. Available: https://www.sciencedirect.com/science/article/pii/S014102961400217X

[13] N. E. A. Nassar, "Corrosion in Marine and Offshore Steel Structures: Classification and Overview," *Int. J. Adv. Eng. Sci. Appl.*, vol. 3, no. 1, p. 7–11, 2022. [Online]. Available: https://www.londontechpress.co.uk/index.php/ijaesa/article/view/80

[14] Y. Sharifi, "Uniform Corrosion Wastage Effects on the Load-Carrying Capacity of Damaged Steel Beams," *Adv. Steel Constr.*, vol. 8, no. 2, pp. 153–167, 2012. [Online]. Available: https://api.semanticscholar.org/CorpusID:252275722

[15] J. R. Galvele, "Pitting Corrosion," in *Corrosion: Aqueous Processes and Passive Films*, ser. Treatise on Materials Science and Technology, J. C. Scully, Ed. Elsevier, 1983, vol. 23, pp. 1–57. [Online]. Available: https://www.sciencedirect.com/science/article/pii/B9780126336702500061

[16] A. G. Poulimenos and J. S. Sakellariou, "A transmittance-based methodology for damage detection under uncertainty: An application to a set of composite beams with manufacturing variability subject to impact damage and varying operating conditions," *Struct. Health Monit.*, vol. 18, no. 1, pp. 318–333, 2018. [Online]. Available: https://doi.org/10.1177/1475921718779190

[17] S. Chesné and A. Deraemaeker, "Damage Localization Using Transmissibility Functions: A Critical Review," *Mech. Syst. Signal Process.*, vol. 38, no. 2, pp. 569–584, 2013. [Online]. Available: https://www.sciencedirect.com/science/article/pii/S0888327013000745